Environmental Science
Processes & Impacts

Fate of Transition Metals in PO4-based in vitro Assays: Equilibrium Modeling and Macroscopic Studies

Journal:	*Environmental Science: Processes & Impacts*
Manuscript ID	EM-ART-09-2020-000405.R2
Article Type:	Paper

Environmental impact

In-vitro assays are used to approximate the oxidative stress that results from particulate matter (PM) exposure by measuring oxidative potential (OP, a proxy for PM toxicity). While these assays have been used extensively to study organic compounds, they are also being used to determine the OP of transition metals. Several OP assays employ phosphate to buffer the system at pH = 7.4 for biological relevance. In this work, we show that oxidation and precipitation of many transition metals, including those present at high concentrations in atmospheric PM, occurs in this buffered phosphate matrix. This raises important questions about the use of such assays to assess PM toxicity.

Fate of Transition Metals in PO_4-based *in vitro* Assays: Equilibrium Modeling and Macroscopic Studies

*Brian. E. Reed, Jayashree Yalamanchili, Jennie. B. Leach, and Christopher. J. Hennigan
Department of Chemical, Biochemical and Environmental Engineering, University of Maryland, Baltimore County, Baltimore, 1000 Hilltop Circle, Maryland, 21250

Corresponding Author: B. E. Reed (reedb@umbc.edu)

Abstract

Transition metals are thought to be among the most toxic components in atmospheric particulate matter (PM) due to their role in catalyzing reactive oxygen species (ROS) formation. We show that precipitation of the transition metals Fe(II), Fe(III), and Mn(II) are thermodynamically favored in phosphate-based assays used to measure the oxidative potential (OP) – a surrogate for toxicity – of PM. Fe and Mn precipitation is likely to occur at extremely low metal concentrations (< 0.5 μM), levels that are imperceptible to the naked eye. The concentration of each metal (other than Cu) in aqueous PM filter extracts often exceeds the solubility limit in OP assays, indicating favorable thermodynamic conditions for precipitation. Macroscopic experimental results at higher metal concentrations (> 100 μM) with visible precipitates provide quasi-validation of the thermodynamic modeling. Oxidation of Fe(II) to Fe(III) is likely to be rapid in all in vitro OP assays, transforming Fe to a much less soluble form. Fe precipitates are likely to increase the rate of precipitation of other metals and possibly induce co-precipitation. These results have direct relevance for all PO_4-based assays; the implications for studies of PM toxicity are discussed.

Introduction

Particulate matter (PM) exerts numerous deleterious effects on human health,[1,2] which contributes significantly to the global burden of disease.[3,4] There is strong evidence that PM induces oxidative stress, and this is hypothesized as a critical link between PM exposure and many adverse health outcomes.[5-8] If true, this implies that the chemical species present in PM have different toxicities, since individual compounds have different reactivities and catalyze or form variable amounts of reactive oxygen species (ROS).

Acellular methods have been widely deployed to approximate the oxidative stress that may result from PM exposure through measurements of oxidative potential (OP). The general approach is to select a compound that reacts with cellular oxidants, and measure its time-dependent decay when exposed to PM extracts. The OP of the sample or matrix scales linearly with the blank-corrected reaction extent in a given time. Because oxidative stress is definitively linked to many disease outcomes, the acellular OP measurements are taken as a proxy for PM toxicity.[9] A variety of OP assays have been developed, including dithiothreitol (DTT),[10] ascorbic acid (AA),[11] and glutathione.[12]

In order to mimic conditions within human lungs, most of the assays are run at 37 °C and pH = 7.4, often using a phosphate buffer to keep the pH constant.[13, 10, 11] However, under these conditions, precipitation, co-precipitation, complexation with PO_4, adsorption and oxidation of metals present in PM (and PM extracts) are thermodynamically possible. The catalytic properties of metals change drastically with phase (solid vs. aqueous), solids composition (e.g., Fe_2O_3(s) vs. Fe_3O_4(s)), and oxidation state.[14, 15] Fe, the transition metal present in ambient PM at the highest concentrations,[16, 17] can form iron-oxides that have a well-known ability to adsorb other soluble metals.[18–20] These phenomena may contribute to some of the inconsistency in

studies characterizing the health effects of specific PM components.[21, 22] DTT consumption rates for organic compounds are widely reported to be linear with the contaminant concentration[23] but for metals the relationship is often reported to be a power law response – the DTT consumption rate levels off at high metal concentrations.[23, 24] Chemical and physical transformations of transition metals may represent a previously unidentified artifact associated with OP assays used as proxies for PM toxicity.

The purpose of this study is to characterize the behavior of several PM metals in PO_4-based *in vitro* incubation fluids using MINEQL thermodynamic software[25] and quasi-validate modeling results using visual observations and metal fate experiments. Cu(II) and Mn(II) were chosen because of their high reactivity in acellular OP assays[23, 24, 26] while Fe(II)/Fe(III) were chosen because they are often present in PM at concentrations an order of magnitude higher than other transition metals.[16, 17] Equilibrium modeling results guide future experimental work on the fate of metals in PO_4-based acellular incubation fluids and the effect of metal precipitation on ROS generation.

Materials and Methods

Modeling Approach: The behavior of the studied metals were assessed as a function of precipitate type, pH, [$TOTPO_4$], [$TOTCO_3$], partial pressure of $O_{2(g)}$ (P_{O2}) and iron-oxide concentration (for the adsorption of metals by iron oxide precipitate). Thermodynamic data (Tables S1-S4, Supplemental Information) contained in MINEQL were supplemented with data from the NIST database as needed.[27] Unless otherwise noted model runs were conducted at pH = 7.4, ionic strength (I) = 0.22 M, total $TOTPO_4$ = 0.1 M, $TOTCO_3$ = 1.4 x 10^{-4} M (closed system), and T = 37 ^{o}C. MINEQL corrects equilibrium constants for ionic strength and temperature using the Davies and Van't Hoff equations, respectively. An ionic strength of 0.22

M is based on the addition of 0.08 M of KH_2PO_4 and 0.02 M of KH_2PO_4 – a common recipe for PO_4-based assays. The effect of $TOTCO_3$ on metal precipitation/complexation was studied by assuming that the phosphate buffer and other reagents had equilibrated with the atmosphere ($P_{CO2} = 10^{-3.5}$ atm) at pH = 7.4 during DI water/reagent storage, and then introduced to the assay incubation tubes (closed system with minimal headspace, T = 37 ºC), resulting in $TOTCO_3 = 1.4x10^{-4}$ M. For the effect of dissolved oxygen, we assumed conditions ranging from very low levels ($logP_{O2} = -0.69$ atm) to saturation ($logP_{O2} = -50$ atm). In Table S5, modeling procedures for each task are presented based on the steps employed in *MINEQL*. The behavior of antioxidants (*e.g.*, DTT) in the metal-PO4 mixtures was not modeled because thermodynamic data (*e.g.*, redox equilibria, stability constants) were not available. In addition, we acknowledge the uncertainty that arises with equilibrium modeling due to: (1) the inherent difference in reported constants, (2) assuming equilibrium conditions for systems that may not be at equilibrium and (3) applying constants determined under specific experimental conditions (metal concentration, temperature and ionic strength) to systems having different conditions.

Macroscopic Experiments: Precipitation and oxidation experiments were conducted to help assess which solids would form in the phosphate buffer, thus quasi-validating the thermodynamic modeling. Stock solutions were prepared using reagent-grade metal salts stored in 2% nitric acid solutions. The metal concentrations in the stock solutions were quantified by ICP-MS (NexION 300D, PerkinElmer). Experiments were conducted at metal concentrations between 5 and 5000 µM in the presence of phosphate buffer (10^{-5} to 0.1 M) and in DI water. PO_4 solutions and DI water were oxygenated prior to use. Samples were prepared and placed in a thermomixer for 30 min at 37 ºC and 400 rpm - conditions used in the DTT assay.[10, 11, 12, 23] Samples were allowed to settle for 10 min after which pictures were taken and a 30 mL aliquot

was passed through a 0.45 μm filter. Aliquots were immediately (<5 min) analyzed for Cu(II), Mn(II), Fe(II), total Fe, and Fe(III) (by difference) using colorimetric methods (HACH, TOTFe: 8008; TOTFe(II): 8146; TOTFe(III) by difference; TOTCu(II): 8143; TOTMn(II): 8149).[28] Interference from the high phosphate levels precluded the use of ICP-MS for metals analysis. Calibration curves were developed for a range of PO_4 concentrations and all curves were linear (Fig. S1, Supporting Information). Most of the macroscopic experiments were conducted in triplicate and all showed a very high degree of reproducibility. The standard deviations of the amount precipitated for each metal are as follows: Fe(III): 2.2%; Fe(II): 2.7%; Cu(II): 1.0%; Mn(II): 1.8 (Table S7, Supporting Information). In Fe(II) oxidation experiments the average standard deviation for Fe(II) and Fe(III) measurements were 0.5 and 2.8, respectively. Macroscopic visual experiments were conducted in the presence of DTT (100 μM) and the absence. DTT did not inhibit precipitation for any of the metals studied (Figs. S2-S5).

Results and Discussion

Precipitate Type: Fe, Cu, and Mn can each form a number of precipitates. Our first goal was to identify the precipitates most likely to form and their corresponding solubility under conditions present in PO_4-based acellular assays. Each precipitate was considered separately in MINEQL - other precipitates were prohibited. In Figure 1, the metal solubility results (total concentration of all aqueous phase metal species) are presented for each precipitate type. All metals formed hydroxides, oxides or PO_4-based precipitates. Aqueous metal concentrations in PM oxidative potential studies typically range from 0.5 μM to ~50 μM [23, 24, 26] and all studied metals had at least one precipitate with a solubility lower than 5 μM. For subsequent modeling tasks we selected one PO_4-based (if one formed) and one non-PO_4 precipitate for each metal/oxidation

state. The chosen precipitates are represented by the cross-hatched bars in Figure 1. For Fe(II) and Mn(II), only PO_4-based precipitates were considered because the solubilities of the

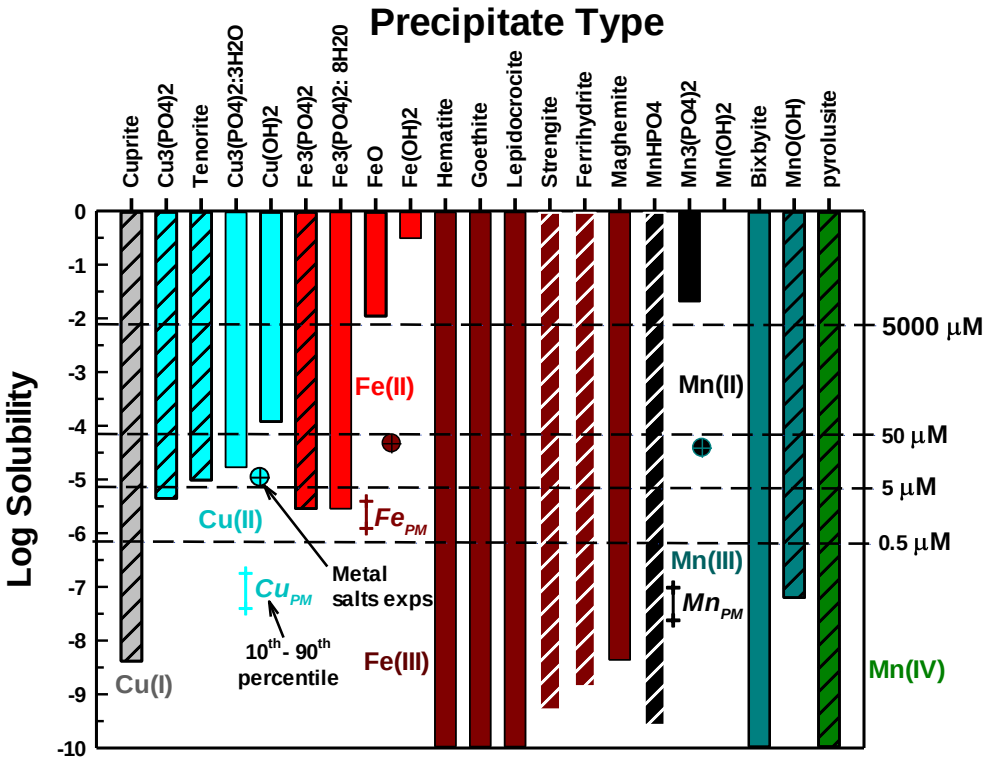

Figure 1. Thermodynamic predictions of metal solubility at pH = 7.4, $TOTPO_4$ = 0.1 M, $TOTCO_3$ = 1.4 x 10^{-4} M, I = 0.22 M and T = 37°C. Cross-hatched bars are solids that were selected for further study. Me_{PM} data represent the 10th to 90th percentile average of urban PM, in conditions of aqueous PM filter extracts. Single cross-hatched data points represent the highest metal concentrations used in metal salt experiments.

oxide/hydroxide precipitates were much higher than the concentration of these metals in PM extracts. Cu(I), Mn(III) and Mn(IV) only form oxide type solids. For Mn(III), manganite ($MnO(OH)_{(s)}$) was selected because iron is a component of bixbyite[29] and Mn(IV) only forms pyrolusite ($MnO_{2(s)}$). For Cu(II), $Cu_3(PO_4)_{2(s)}$ and tenorite ($CuO_{2(s)}$) were chosen because at 5 µM TOTCu a precipitate formed (the remaining Cu precipitates have solubilities > 5 µM).

Selecting which nonPO_4-based Fe(III) solid was most likely to form was more difficult because of the large number of potential precipitates. For reasons discussed in detail below, we chose strengite ($FePO_4$-$2H_2O$) and ferrihydrite ($Fe(OH)_{3(s)}$). Rather than use the terms "iron-oxide-like" or "iron-PO_4-like" (or "Mn/Cu-oxide-like" or "Mn/Cu-PO_4-like") to denote newly formed precipitates, we choose to use the crystalline name with the caveat that the precipitates are likely in the amorphous form. In addition, solubility products (K_{S0}) for amorphous solids are not readily available and we acknowledge that using K_{S0} for crystalline precipitates will result in a lower predicted solubility compared to the amorphous solids. For all metals, carbonate-based solids and complexes were not present. The behavior of Fe(II) and Fe(III) will be discussed together because Fe(II) is predicted to rapidly oxidize to Fe(III) under these conditions.

MINEQL runs were conducted with precipitation allowed and prevented – conditions that represent the two extreme possible behaviors in PO_4-based assays (Fig. S7). For the runs where precipitation was allowed, the precipitates described above (hatched bars in Fig. 1) were included in the model runs allowing for the most thermodynamically favored solid to form. The dominant species predicted for all simulation conditions are given in Table S6.

The Me_{PM} data in Figure 1 represent the 10^{th} to 90^{th} percentile average annual metal concentrations measured for ten urban areas across the US[17] determined using well-established PM filter sampling and extraction protocols (e.g., following the approach of Verma et al., 2014).[30] Note Me_{PM} data represent total metal concentrations, *i.e.*¸ there was no differentiation between metal oxidation states. The single cross-hatched data points represent some metal concentrations examined in studies where metals were added as salts, shown for reference.[23, 24, 26] Total Fe_{PM} data averaged 2.3 µM and 10^{th} to 90^{th} percentile concentrations were 1.24 and 4.0 µM, respectively. The highest Fe(III) and Fe(II) concentrations used in metal salt studies were

47 and 10 µM, respectfully. As discussed above, any aqueous Fe(II) is likely to be rapidly oxidized to Fe(III), and all five Fe(III) compounds considered here have solubilities that are orders of magnitude lower than the range of concentrations in filter extracts from PM sampled in urban areas. This strongly suggests that aqueous Fe in PM extracts, even for samples that represent low atmospheric concentrations as well as those used in metal salt studies, will rapidly precipitate in PO_4-based assays. Cu_{PM} data averaged 0.06 µM while the 10^{th} to 90^{th} percentile concentrations were 0.04 and 0.18 µM, respectively. The highest Cu(II) concentrations used in metal salt studies was 11 µM. Cu_{PM} is well below the solubility limit for all Cu(II) species considered; therefore, precipitation of aqueous Cu in PO_4-based assays of PM toxicity is not likely. However, Cu(II) precipitation could occur in metal salt experiments if TOTCu(II) > 4.47 µM (solubility of $Cu_3(PO_4)_{2(s)}$). While Cu(I) is highly insoluble, the redox conditions in the OP assays are oxidizing due to the presence of dissolved oxygen, suggesting that reduction of Cu(II) to Cu(I) and subsequent precipitation is unlikely. However, if Cu was present as Cu(I), precipitation is possible if Cu(I) is not oxidized to Cu(II). Mn_{PM} data averaged 0.058 µM while the 10^{th} to 90^{th} percentile concentrations were 0.024 to 0.098 µM, respectively. The highest Mn(II) concentration from metal salt studies was 39 µM. If Mn exists as Mn(II) and is not oxidized, Mn(II) precipitation is not predicted to occur. However, if Mn is present as Mn(III) or Mn(IV), or if Mn(II) is oxidized, then precipitation of aqueous Mn in PO_4-based assays is thermodynamically favored.

The effect of K_{so} ($\log K_{so} \pm 2$) on metal solubility was conducted for the selected precipitates to access the uncertainty in published values of K_{so} (Fig S6). Tenorite was most affected by the value of K_{so}, followed by $Cu_3(PO_4)_{2(s)}$, $Fe_3(PO_4)_{2(s)}$ and $MnO(OH)_{(s)}$. The remaining precipitates had solubilities well below 5 µM (the lowest metal concentration investigated).

In summary, precipitation of Fe and Mn is likely in PM filter extracts originating from urban areas and in metal salt studies. Cu(II) precipitation in PO_4-based assays is unlikely for PM extracts, but may occur in metal salt experiments if the total Cu(II) concentration exceeds 4.47 µM.

In the following sections, we discuss in detail the modeling results for each metal, focusing on the effects of pH, $TOTPO_4$, carbonate, and dissolved O_2. We present the macroscopic experimental results, including the visual presence/absence of precipitates and chemical analysis of dissolved metals. We acknowledge that the high metal concentrations used to visually observe precipitation do not represent metal concentrations in PM extracts unless samples were taken from heavily polluted areas or for extended periods of time. However, detection of precipitates at concentrations typical of PM extracts is challenged by the extremely low mass present. For example, 15 mL of Hi-Vol filter extract following the procedure of Verma et al. [30] contains approximately ~2-8 x 10^{-8} g of Mn (range representing urban concentrations in the US).[16] Creative experimental approaches combined with advanced analytical techniques are required to physically detect precipitates at such low levels: this is the topic of ongoing work by our group. Therefore, we believe that the macroscopic experimental results are useful in understanding what can occur thermodynamically in PO_4-based assays in regards to precipitation, oxidation and changing assay conditions (*e.g.*, effect of $TOTPO_4$).

Iron: Fe(II) formed $Fe_3(PO_4)_{2(s)}$ and Fe(III) formed strengite or ferrihydrite depending on the magnitude of $TOTPO_4$ (Fig. 2a). Based on visual observations and the aqueous phase Fe(III) analysis, we are confident that strengite formed at higher $TOTPO_4$/TOTFe ratios (Fig 2). Hsu (1982) [31] reported that phosphate induces nearly immediate formation of a fluffy "whitish" precipitate, with ~98% of the Fe(III) in the precipitate at equilibrium. In a similar aqueous matrix, Senn et al. (2015) [32] reported amorphous $FePO_{4(s)}$ formation, which appeared beige in color. Senn et al. (2015) [32] also observed shifting precipitate identity as a function of the $TOTPO_4$/TOTFe molar ratio: the Fe(III) suspension changed from "whitish" to an "orange" or "brownish" as $TOTPO_4$/TOTFe decreased, indicating the formation of lepidocrocite (orange) or ferrihydrite (brown). We observed similar behavior in our experiments (Fig. 2b) - the type of solid clearly changed from beige ($FePO_{4(s)}$) to

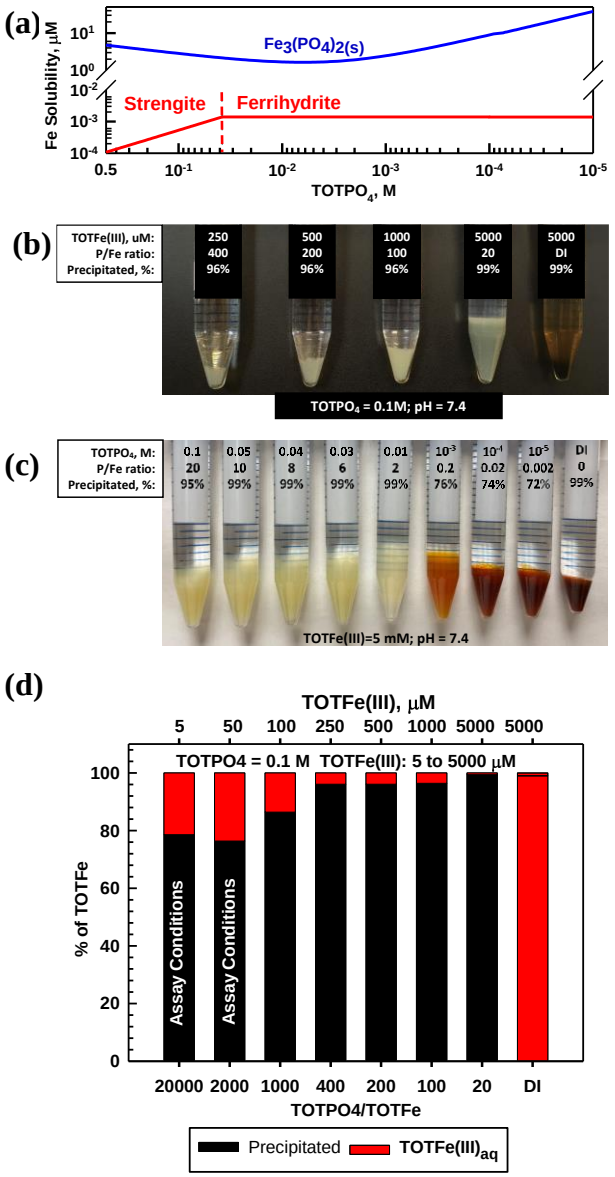

Figure 2. Equilibrium modeling and macroscopic results: (a) thermodynamic predictions of Fe(III) and Fe(II) solubility as function of $TOTPO_4$; (b) macroscopic experimental results, including visual observations at $TOTPO_4$ = 0.1 M, with varying TOTFe(III); (c) macroscopic experimental results, with visual observations at TOTFe(III) = 5 mM, varying $TOTPO_4$ and (d) precipitation results for varying TOTFe(III), $TOTPO_4$ = 0.1 M. Note, in (b), (c), and (d) the percent of Fe precipitated is based upon chemical analysis.

orange-brown between 0.01 and 0.001 M $TOTPO_4$ (initial Fe constant at 5 mM). When lepidocrocite and strengite are both allowed to form in MINEQL, 100% of the Fe(III) exists as lepidocrocite (Fig. S8), which does not match what we observed visually. Ferrihydrite and maghemite form at $TOTPO_4$ less than 0.037 M and 0.011 M, respectively. While maghemite formation matched the visual pattern better than ferrihydrite (Fig. S9), we selected ferrihydrite because Singh et al. (2010) [33] reported that the precipitation of ferrihydrite is favored when hydrolysis occurs rapidly and ferrihydrite formation in the presence of PO_4 was reported by Senn et al. (2015).[32]

At 0.1M $TOTPO_4$/pH = 7.4 (conditions used in most PO_4-based acellular assays) precipitation of Fe(III) was observed visually over a wide range of TOTFe(III) (Fig. 2c). While we did not observe visible solid formation at low TOTFe(III) (a 10 mL solution of 50 μM Fe contains only 2.8×10^{-5} g of total Fe), precipitation was confirmed based on chemical analysis of filtered samples (Fig 2d). Note, we confirmed that neither PO_4 nor DTT interfere with the Fe measurements. At 50 μM TOTFe(III), 77% of added Fe(III) precipitated, while 86-99% of Fe precipitated at higher TOTFe(III). Decreased precipitation at lower TOTFe(III) could be due to the presence of small strengite-type particles that escape filtration.[34] The remaining aqueous Fe(III) exists as $Fe(OH)_2^+$ and $Fe(OH)_{3(aq)}$ (Table S6).

Fe(III) (as well as Fe(II), Cu(II) and Mn(II)) precipitation occurred experimentally at all TOTFe(III)-$TOTPO_4$ combinations within the 30 min duration of acellular assays. Precipitation is a two-step process of nucleation and crystal growth, with nucleation typically the rate-limiting step.[35] Nucleation can be considered homogenous (slow, random particle growth) and heterogeneous (fast, nucleation occurs on existing surfaces). To date, there have been no kinetic studies of $FePO_{4(s)}$ growth under PO_4-based acellular conditions. However, Senn et al. [32] and

Madsen and Koch [34] investigated the formation of $FePO_{4(s)}$ following the oxidation of Fe(II) to Fe(III). Senn et al. [32] conducted macroscopic studies and reported that within 6 min, a beige "Fe(III)-phosphate precipitate" formed after Fe(II) addition. At $TOTPO_4/TOTFe < 0.52$, the suspension color changed from initially beige to orange over 240 min indicating that the formation of $FePO_{4(s)}$ occurred first, followed by $FePO_{4(s)}$ dissolution and then the formation of Fe(III)-oxide precipitate. While we did not observe this time-dependent transition, we did observe the apparent shift from Fe(III)-phosphate precipitate to Fe(III)-oxide precipitate at a similar P/Fe ratio (between 0.2-2 in our work).

It is highly likely that Fe(III)-oxide solid would form in acellular assays at lower $TOTPO_4$, suggesting that decreasing the phosphate buffer concentration would not prevent Fe(III) precipitation. Grundl and Delwiche [36] reported that ferric iron precipitation in the absence of phosphate was first order with respect to $Fe(OH)_{3(aq)}$: $dFe(III)/dt = -k[Fe(OH)_{3(aq)}]$. The precipitation rate decreased with increasing TOTFe(III) concentration (half-lives: 5 min and 15 min at TOTFe(III)=500 and1000 μM, respectively) due to the poisoning of the surface by Fe^{3+} and to a lesser extent by $Fe(OH)^{2+}$. Grundl and Delwiche's work was conducted at pH 2.5 – 3 where $Fe^{3+}/Fe(OH)^{2+}$ are dominant, while at pH = 7.4 $Fe^{3+}/Fe(OH)^{2+}$ are essentially nonexistent. As with the other metals, our goal with this work is to characterize the predicted metal phase state and speciation in the PO_4 matrix. Connecting the formation of metal-complexes and precipitates with the generation of ROS or the response of OP assays is beyond the scope of this study, but warrants attention. Metals can catalyze ROS formation in solid or aqueous form [37] therefore, it is likely that the formation of precipitates could also affect the DTT consumption rate.

The effect of $[O_{2(aq)}]$ on metal oxidation was investigated by varying the O_2 partial pressure from 0.21 to essentially zero (at 25°C and P_{O2} = 0.21 atm, $[O_{2(g)}] \approx 275$ μM, 8.9 mg/L). Fe(II) is oxidized to Fe(III) at very low $[O_2]$ concentrations (Fig S10). Fe(II) and Fe(III) either form $Fe_3(PO_4)_{2(s)}$ or strengite, respectively, depending on the P_{O2} level. Sung and Morgan [38] summarized results from multiple studies on the kinetics of Fe(II) to Fe(III) oxidation in the natural environment. Half-lives ranged from ~ 16-47 min at pH levels between 6.3-6.52 and ~ 3.3-5.5 min at pH = 8.0. Madsen and Koch [34] reported that Fe(II) was oxidized in water with very low dissolved oxygen (DO) concentrations (H_2O purged with $N_{2(g)}$) and that iron phosphate solid catalyzed Fe(II) oxidation. These results indicate the likely rapid transformation of Fe(II) to Fe(III) during any *in vitro* measures of PM toxicity with phosphate in the assay matrix.

In our experiments, Fe(II) formed a whitish precipitated at $TOTPO_4 \geq 0.01$ M, transitioned to a grayish-white precipitate at $TOTPO_4 = 10^{-3}$ M, and then to an orange/brown precipitate at $TOTPO_4 \leq 10^{-4}$ M (Fig 3a). For $TOTPO_4$/TOTFe(II) combinations in which a whitish precipitate was observed, it is not possible to say if $Fe_3(PO_4)_{2(s)}$ or strengite formed. However, when the orange/brown precipitates were present, it is clear that Fe(II) was oxidized to Fe(III) with subsequent Fe(III)-oxide solid formation. $FeO_{(s)}$ or $Fe(OH)_{2(s)}$ solid formation was not possible given their very high solubilities ($FeO_{2(s)}$ – 0.011 M; $Fe(OH)_{2(s)}$ – 0.31 M, Fig. 1). Fe(II) oxidation to Fe(III) is further demonstrated in the Fe(II)-DI water experiments, where ferrihydrite formed following Fe(II) oxidation to Fe(III). Chemical analysis of filtered samples also reinforces this observation – at $TOTPO_4$/TOTFe(II) $\leq$ 0.2 and in DI water there was a mixture of Fe(II)/Fe(III) in the aqueous phase.

For $TOTPO_4$ = 0.1 M a whitish precipitate formed at TOTFe(II) = 250 to 5000 μM (Fig. 3c). At 50 μM and 100 μM TOTFe(II) there was no visual precipitation but 7.9% and 11.4% of the

(a)

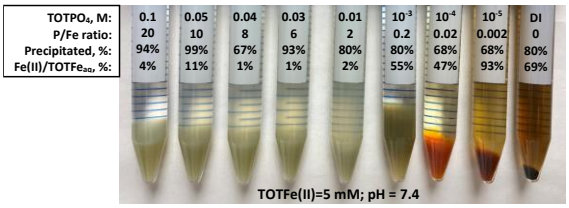

(b)

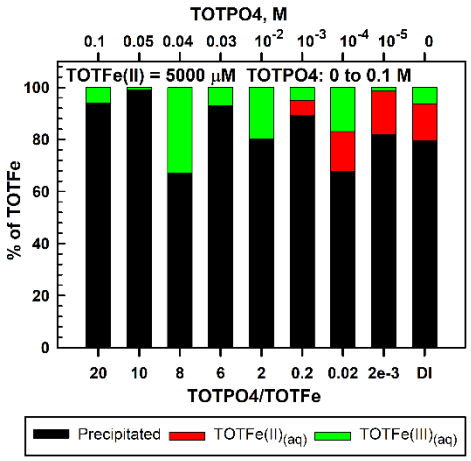

(c)

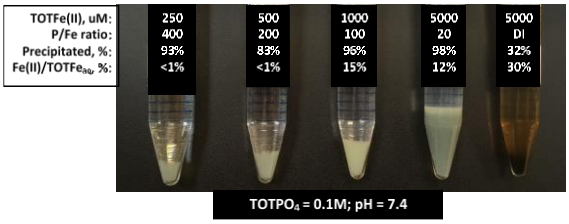

(d)

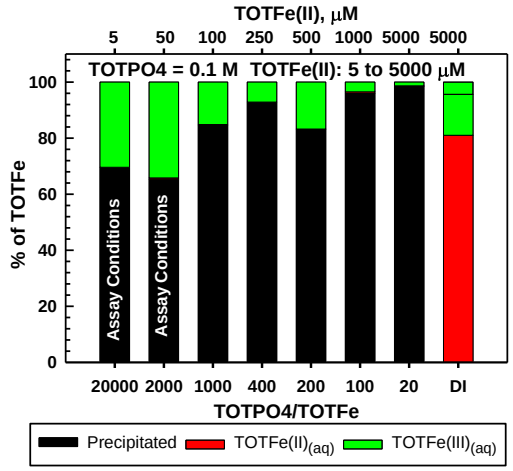

Figure 3. Fe(II) Macroscopic results: a) visual observations at TOTFe(II) = 5 mM, varying $TOTPO_4$; (b) precipitation/oxidation results at TOTFe(II) = 5 mM, varying $TOTPO_4$; (c) visual observations at $TOTPO_4$ = 0.1 M, varying TOTFe(II) and (d) and precipitation/oxidation results at $TOTPO_4$ = 0.1 M, varying TOTFe(II). Note all results in Figure 3 are based on chemical analyses.

total iron precipitated as either $Fe_3(PO_4)_{2(s)}$ or strengite. At the lower TOTFe(II) there was significant oxidation of Fe(II) to Fe(III) based on analysis of filtered samples (Fig 3d) but it is unclear why more Fe(III) did not precipitate as strengite. Under similar conditions for TOTFe(III) = 50 and 100 μM there was more precipitation of Fe(III) but still a significant amount of Fe(III) in solution relative to higher TOTFe(III) concentrations (Fig. 2d). It is possible that the combination of Fe(II) oxidation to Fe(III) and Fe(III) precipitation to strengite were subject to slower kinetics than that observed at higher iron concentrations. Under PO_4-based in vitro assay conditions (indicated in Fig 3d) Fe(II) was oxidized and there was precipitation of either $Fe_3(PO_4)_{2(s)}$ or strengite (or both). Oxidation of Fe(II) to Fe(III) is highly likely to occur, though the identity of the specific solids is based upon specific conditions within the assay and we can speculate that these transformations will likely affect the generation of ROS in PO_4-based assays.

Copper: At pH = 7.4 Cu(II) exists predominantly as $CuHPO_{4(aq)}$ (Fig. 4a and Tab. S7). At slightly higher pH (> 7.6), tenorite is predicted to form over $Cu_3(PO_4)_{2(s)}$ (Fig. S7). For TOTCu(II) ≤ 250 μM at $TOTPO_4$ = 0.1 M/pH = 7.4 there was no visible precipitate formation (Fig 4b); however, the aqueous Cu measurements indicate that precipitation did occur (Fig. 4d). At $TOTPO_4 \geq 0.14$ M all Cu(II) exists as $CuHPO_{4(aq)}$; for $TOTPO_4$ between 0.14 and 0.03 M $Cu_3(PO_4)_{2(s)}$ forms, while tenorite forms below 0.03 M $TOTPO_4$ (Fig. 4a). Matching visual observations to equilibrium modeling results is more difficult with Cu(II) because there were no changes in precipitate appearance (the deeper blue precipitates could be due to density differences of the settled solids). Cu(II) precipitation occurred experimentally at all TOTCu(II)-$TOTPO_4$ combinations within the 30 min duration of in vitro assays. For all macroscopic experiments at $TOTPO_4$ = 0.1 M/pH = 7.4, the measured $TOTCu_{(aq)}$ was always greater than the

predicted Cu(II) solubility (4.47 μM). Cu(I) in the acellular assay matrices would exist as aqueous Cu(I) or $CuO_{2(s)}$ (Fig. S10) or be oxidized to Cu(II). It is interesting to note that Cu(II) is reported to be the most active of the transition metals in generating ROS[23], which could in part be due to its high solubility.

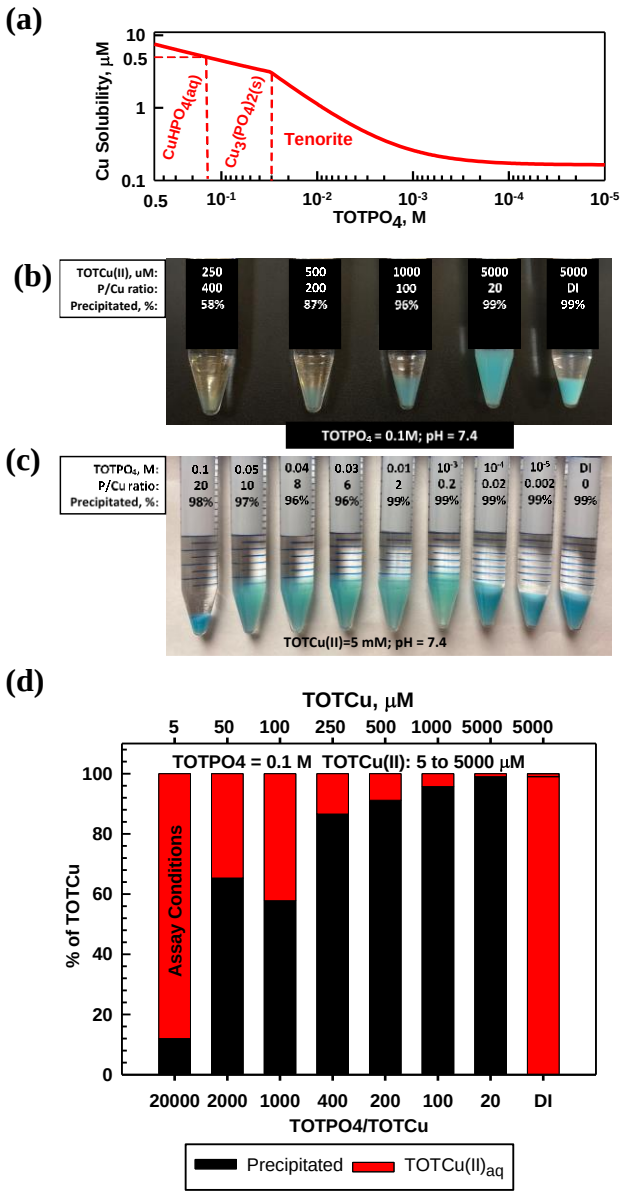

Figure 4. Cu(II) Equilibrium modeling and macroscopic results: (a) thermodynamic predictions of Cu(II) solubility as function of $TOTPO_4$; (b) macroscopic experimental results, including visual observations at $TOTPO_4$ = 0.1 M, varying TOTCu(II); (c) macroscopic experimental results, including visual observations at TOTCu(II) = 5000 μM, varying $TOTPO_4$ and (d) precipitation results for varying TOTCu(II), $TOTPO_4$ = 0.1 M. Note, in (b), (c), and (d) the percent of Cu precipitated is based upon chemical analysis.

Manganese: Mn proved to be the most complicated of the metals studied because of its multiple oxidation states and precipitates. At $TOTPO_4$ = 0.1 M/pH = 7.4 Mn(II) exists as $MnHPO_{4(aq)}$ (95%; no precipitation, Tab. S7) or $MnHPO_{4(s)}$ (Fig. 5a). Mn(III) exists as Mn^{3+} or $MnO(OH)_{(s)}$ (Tab. S7). Mn(IV), a highly insoluble species ($MnO_{2(s)}$ solubility = 2.3 x10^{-13} M), does not form complexes with OH^- or PO_4. At TOTMn(II) ≥ 500 µM and $TOTPO_4$ = 0.1 M a whitish precipitate formed (Fig. 5b) while at lower TOTMn(II) precipitation was demonstrated by measuring the Mn concentration in filtered samples (Fig. 5d). When precipitation was studied as a function of $TOTPO_4$, a whitish precipitate formed at $TOTPO_4 \geq 0.01$ M and a brownish/black precipitate at $TOTPO_4 \leq 10^{-3}$ M (Fig. 5c). If we assume the whitish precipitate is $MnHPO_{4(s)}$ then clearly a different solid formed at lower $TOTPO_4$. If $MnHPO_{4(s)}$ formation does not occur, the

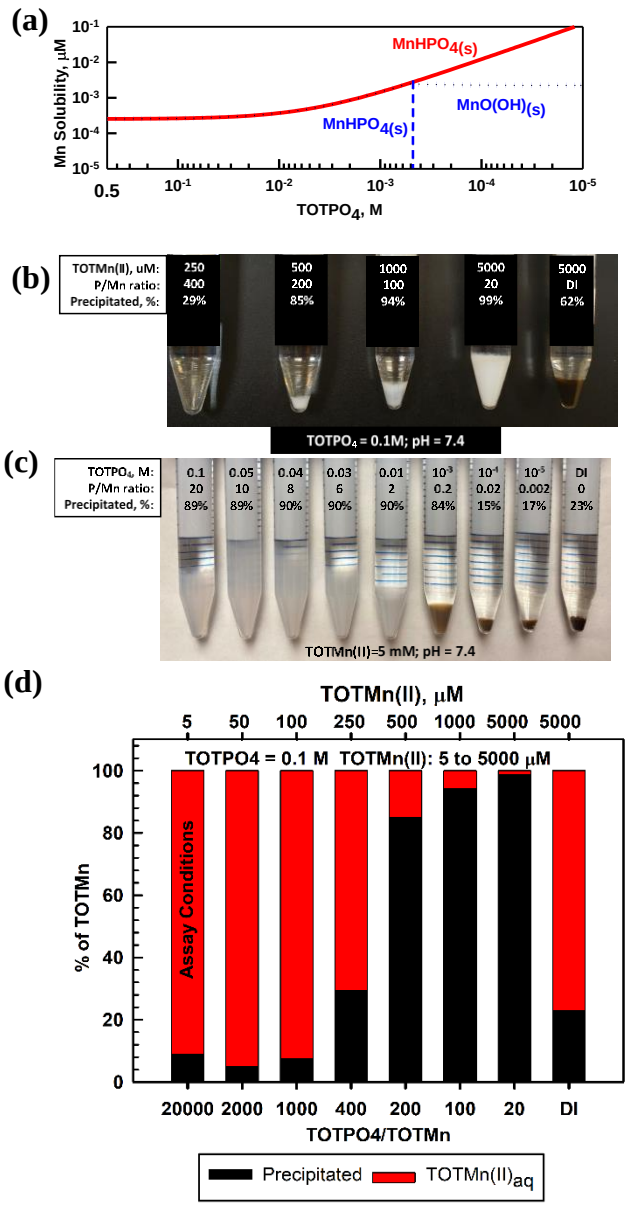

Figure 5. Mn(II) Equilibrium modeling and macroscopic results: (a) thermodynamic predictions of Mn(II) solubility as function of $TOTPO_4$; (b) macroscopic experimental results, including visual observations at $TOTPO_4$ = 0.1 M, varying TOTMn(II) ; (c) macroscopic experimental results, including visual observations at TOTMn(II) = 5000 µM, varying $TOTPO_4$ and (d) precipitation results varying TOTMn(II), $TOTPO_4$ = 0.1 M. Note, in (b) (c), and (d) the percent of Mn precipitated is based upon chemical analysis.

remaining two Mn(II) precipitate solubilities ($Mn_3(PO_4)_{2(s)}$ (0.02 M) and $Mn(OH)_{2(s)}$ (2.07 M) (Fig. 1)) are far higher than what we measured.

Redox transformations of dissolved Mn are likely in PO_4-based matrices, though the speciation of Mn is uncertain. Mn(II) can be oxidized to Mn(III) or Mn(IV) under lower DO concentrations with the subsequent formation of $MnO(OH)_{(s)}$ or $MnO_{2(s)}$ (Fig. S10). Stumm and Morgan [35] reported an Fe(II)-type oxidation relationship for Mn(II) to Mn(IV): $d[Mn^{2+}]/dt = -k[OH^-]P_{O2}[Mn^{2+}]$ with the Mn(II) oxidation rate very low at pH < 9. The oxidation rate may be higher in PO_4-based assays due to the higher temperature and higher $[O_2]$ (assuming reagents are in equilibrium with the atmosphere). However, the formation of $MnHPO_{4(aq)}$ complexes could slow the Mn(II) oxidation rate. Faust and Aly [39] reported that Mn(II) oxidization is catalyzed by $MnO_{2(s)}$ and it is possible that $MnHPO_{4(s)}$ may catalyze the Mn(II)→Mn(IV) reaction but there are no literature results to confirm this mechanism. A more likely scenario is that Mn(II) is oxidized to Mn(III) with the formation of $MnO(OH)_{(s)}$ – at lower TOTPO4 we observe that the formation of the brown/blackish precipitate occurs experimentally at $TOTPO_4 \approx 10^{-3}$ M (Fig 5b) and $MnO(OH)_{(s)}$ is predicted to form at $TOTPO_4 = 5x10^{-4}$ M (dotted blue line in Fig 5a).

Adsorption by ferric iron precipitates: Adsorption of metals by iron oxides is a well-known phenomenon. In this task we investigated the adsorption of Cu(II) and Mn(II) onto hydrous ferric oxide (HFO) using the modeling approach of Dzombak and Morel.[20] Fe(III) only forms ferrihydrite at $TOTPO_4 < 0.037$ M (Fig. 2a), thus HFO adsorption modeling is only applicable at phosphate concentrations much lower than what are currently used in OP assays. At 50 μM Fe(III) (all of which was assumed to form HFO) there was minimal adsorption of Cu(II) and Mn(II) (Fig. S11). Senn et al.[32] reported that freshly formed $FePO_{4(s)}$ is capable of adsorbing metals, although there is no experimental data available to quantify $FePO_{4(s)}$ adsorption capacity.

Iron oxide can adsorb orthophosphate [40] and it is possible that $FePO_{4(s)}$ will also adsorb PO_4. Given the high $TOTPO_4$ used in OP assays we believe that PO_4 will out-compete PM metals for adsorption sites and thus metal adsorption is likely of minimal concern.

Conclusions

Overall, the processes we report likely have profound importance for *in vitro* assays of PM toxicity. The results also inform prior studies of transition metal toxicity. Charrier et al.[23] and Fujitani *et al*. [24] reported DTT consumption rate series as:

$$Cu(II) > Mn(II) >> Fe(III) \sim Fe(II) \qquad [24]$$

$$Ni(II) > Cu(II) > Mn(II) > Fe(III) \qquad [25]$$

It is likely that Fe(III) and Fe(II), either added as a reagent or through collected PM, will precipitate in PO_4-based assays: Fe(III) precipitates as strengite and Fe(II) precipitates as $Fe_3(PO_4)_{2(s)}$. Fe(II) is readily oxidized to Fe(III) with subsequent precipitation of Fe(III). Mn(II) precipitates as $MnPO_{4(s)}$ but the precipitation rate appears to be slow at Mn(II) concentrations present in PM extracts (< 5 μM), a possible reason for the high ROS generation potential of Mn(II). Mn(II) oxidation to Mn(IV) is slow at pH < 9 so a more likely scenario is that Mn(II) is oxidized to Mn(III) with subsequent formation of $MnO(OH)_{(s)}$. It is notable that Cu is – by far – the most active metal in catalyzing DTT reaction.[24] The ascorbic acid assay is also highly sensitive to Cu.[11, 41] If these measurements are surrogates for ROS generation in human lungs, then this implies that Cu possesses an enhanced toxicity compared to other metals present in PM.[42] However, toxicological [43] and epidemiological studies [44, 45] generally do not support this assessment. This apparent disconnect is possibly due to its high solubility (~90% solubility at pH = 7.4, $TOTPO_4$ = 0.1 M, TOTCu(II) = 5 μM).

Metal precipitation is highly likely in most assay matrices due to the high $TOTPO_4$ (~0.1-0.5 M) and near-neutral pH (7.4) used to mimic biological systems. Decreasing $TOTPO_4$ in acellular assays (while still maintaining pH = 7.4) shifts the precipitate identity to favor the formation of oxide/hydroxide solids, while still allowing oxidation of Fe(II) and Mn(II). When actual PM material is evaluated in PO_4-based assays, multiple metals will be present increasing the likelihood of co-precipitation and increased precipitation rates (*e.g.,* Fe(III) readily precipitates and then is a source of nucleation sites for other metal precipitates).

On the one hand, this behavior is unsurprising since a defining characteristic of metals is their pH-dependent solubility and their known complexation chemistry with PO_4. However, this phenomenon has not been reported previously, likely because precipitate formation occurs even at low concentrations where solids are most likely colloidal in size and imperceptible to the human eye. Factors such as PM sample matrix, metal concentrations, and metal oxidation state can produce variability in metal precipitation (both rate and amount formed) suggesting that the process we report is quite variable within and between assays. Future studies should extend our results to include thermodynamic and experimental characterization of other PM metals, e.g., V and Ni, in PO_4-based matrices.

The current study informs the fate and transformation of metals in OP assays that achieve pH control (typically pH = 7.4) using phosphate buffers. These include DTT, glutathione, and ascorbic acid. Our results likely extend to simulated (or surrogate) lung fluid (SLF), an acellular medium used to represent conditions in the human respiratory tract.[13, 46] The behavior and fate of metals in cellular assays is unknown, due to interactions between metals and cell culture media, especially organic molecules likely to form complexes with metals (e.g., proteins).

It is important to note that the effects of this phenomenon on assay response (e.g., ROS generation or antioxidant depletion) are beyond the scope of the present study and have not been characterized. Metals in solid and aqueous form can induce ROS formation,[15, 37] but it is likely that these would elicit quite different responses due to their different chemical forms and the surface effects associated with precipitates. For example the presence of antioxidants could facilitate rapid redox cycling of Fe(II)/Fe(III), Mn(II)/Mn(III)/Mn(IV), etc. Additionally, the formation of precipitates could affect the formation of hydroxyl radicals, superoxide and H_2O_2. We recommend that the effects of metal precipitation on ROS formation and differences in assay response to different chemical forms of each metal represent urgent research needs in understanding the health effects of PM and toxicity of individual PM constituents.

Acknowledgments

This work was funded by the National Science Foundation through award #1802474.

We acknowledge Bill Schecher, Chief Programmer, *MINEQL*, for technical assistance with MINEQL, and Aidan Mucci and Carlos Castillo Lara: Undergraduate Research Assistants, UMBC Department of Chemical, Biochemical and Environmental Engineering for assistance with laboratory assays.

Data Availability

All model inputs and outputs have been published, and are freely available at http://hdl.handle.net/11603/18201

Disclosure

The authors declare no competing financial interest.

References

1. Davidson, C.; Phalen, R.; Solomon, P. Airborne Particulate Matter And Human Health: A Review. *Aerosol Science and Technology* 2005, **39 (8)**, 737-749
2. Pope, C.; Dockery, D. Health Effects of Fine Particulate Air Pollution: Lines That Connect. *Journal of the Air & Waste Management Association* 2006, **56 (6)**, 709-742.
3. Institute, H.E., Health Effects Institute, *State of Global Air* 2019.
4. Liu, C.; Chen, R.; Sera, F.; Vicedo-Cabrera, A.; Guo, Y.; Tong, S.; Coelho, M.; Saldiva, P.; Lavigne, E.; Matus, P.; Valdes Ortega, N.; Osorio Garcia, S.; Pascal, M.; Stafoggia, M.; Scortichini, M.; Hashizume, M.; Honda, Y.; Hurtado-Díaz, M.; Cruz, J.; Nunes, B.; Teixeira, J.; Kim, H.; Tobias, A.; Íñiguez, C.; Forsberg, B.; Åström, C.; Ragettli, M.; Guo, Y.; Chen, B.; Bell, M.; Wright, C.; Scovronick, N.; Garland, R.; Milojevic, A.; Kyselý, J.; Urban, A.; Orru, H.; Indermitte, E.; Jaakkola, J.; Ryti, N.; Katsouyanni, K.; Analitis, A.; Zanobetti, A.; Schwartz, J.; Chen, J.; Wu, T.; Cohen, A.; Gasparrini, A.; Kan, H. Ambient Particulate Air Pollution And Daily Mortality In 652 Cities. *New England Journal of Medicine* 2019, **381 (8)**, 705-715.
5. Maher, B.; Ahmed, I.; Karloukovski, V.; MacLaren, D.; Foulds, P.; Allsop, D.; Mann, D.; Torres-Jardón, R.; Calderon-Garciduenas, L. Magnetite Pollution Nanoparticles In The Human Brain. *Proceedings of the National Academy of Sciences* 2016, **113 (39)**, 10797-10801.
6. Wang, T.; Chiang, E.; Moreno-Vinasco, L.; Lang, G.; Pendyala, S.; Samet, J.; Geyh, A.; Breysse, P.; Chillrud, S.; Natarajan, V.; Garcia, J. Particulate Matter Disrupts Human Lung Endothelial Barrier Integrity Via ROS- And P38 MAPK–Dependent Pathways. *American Journal of Respiratory Cell and Molecular Biology*2010, **42 (4)**, 442-449.
7. Schaumann, F.; Borm, P.; Herbrich, A.; Knoch, J.; Pitz, M.; Schins, R.; Luettig, B.; Hohlfeld, J.; Heinrich, J.; Krug, N. Metal-Rich Ambient Particles (Particulate Matter2.5) Cause Airway

Inflammation In Healthy Subjects. *American Journal of Respiratory and Critical Care Medicine* 2004, **170 (8)**, 898-903.

8. Wood, L.; Gibson, P.; Garg, M. Biomarkers Of Lipid Peroxidation, Airway Inflammation And Asthma. *European Respiratory Journal* 2003, **21 (1)**, 177-186.
9. Li, N.; Sioutas, C.; Cho, A.; Schmitz, D.; Misra, C.; Sempf, J.; , M.; Oberley, T.; Froines, J.; Nel, A. Ultrafine Particulate Pollutants Induce Oxidative Stress And Mitochondrial Damage. *Environmental Health Perspectives* 2003, **111 (4)**, 455-460.
10. Cho, A.; Sioutas, C.; Miguel, A.; Kumagai, Y.; Schmitz, D.; Singh, M.; Eiguren-Fernandez, A.; Froines, J. Redox Activity Of Airborne Particulate Matter At Different Sites In The Los Angeles Basin. *Environmental Research* 2005, **99 (1)**, 40-47.
11. Janssen, N.; Yang, A.; Strak, M.; Steenhof, M.; Hellack, B.; Gerlofs-Nijland, M.; Kuhlbusch, T.; Kelly, F.; Harrison, R.; Brunekreef, B.; Hoek, G.; Cassee, F. Oxidative Potential Of Particulate Matter Collected At Sites With Different Source Characteristics. *Science of The Total Environment* 2014, **472**, 572-581.
12. Strak, M.; Janssen, N.; Godri, K.; Gosens, I.; Mudway, I.; Cassee, F.; Lebret, E.; Kelly, F.; Harrison, R.; Brunekreef, B.; Steenhof, M.; Hoek, G. Respiratory Health Effects Of Airborne Particulate Matter: The Role Of Particle Size, Composition, And Oxidative Potential—The RAPTES Project. *Environmental Health Perspectives* 2012, **120 (8)**, 1183-1189.
13. Calas, A.; Uzu, G.; Martins, J.; Voisin, D.; Spadini, L.; Lacroix, T.; Jaffrezo, J. The Importance Of Simulated Lung Fluid (SLF) Extractions For A More Relevant Evaluation Of The Oxidative Potential Of Particulate Matter. *Scientific Reports* 2017, **7 (1)**.

14. Teja, A.; Koh, P. Synthesis, Properties, And Applications Of Magnetic Iron Oxide Nanoparticles. *Progress in Crystal Growth and Characterization of Materials* 2009, *55* (1-2), 22-45.

15. Nico, P.; Kumfer, B.; Kennedy, I.; Anastasio, C. Redox Dynamics Of Mixed Metal (Mn, Cr, And Fe) Ultrafine Particles. *Aerosol Science and Technology* 2009, **43 (1)**, 60-70.

16. Hennigan, C.; Mucci, A.; Reed, B. Trends In PM 2.5 Transition Metals In Urban Areas Across The United States. *Environmental Research Letters* 2019, **14 (10)**, 104006.

17. Vidrio, E.; Jung, H.; Anastasio, C. Generation Of Hydroxyl Radicals From Dissolved Transition Metals In Surrogate Lung Fluid Solutions. *Atmospheric Environment* 2008, **42 (18)**, 4369-4379.

18. Venkataramani, B.; Venkateswarlu, K.; Shankar, J. Sorption Properties Of Oxides. *Journal of Colloid and Interface Science* 1978, **67 (2)**, 187-194.

19. Dempsey, B.; Singer, P. The Effect Of Calcium On The Adsorption Of Zinc By Mnox (S) And Fe(OH)3 (Am). *Journal of Colloid and Interface Science* 1980, **79**, 209-221.

20. Dzombak, D.; Morel, F. *Surface complexation modeling*; Wiley: New York, 1990.

21. Chen, L.; Lippmann, M. Effects Of Metals Within Ambient Air Particulate Matter (PM) On Human Health. *Inhalation Toxicology* 2009, **21 (1)**, 1-31.

22. Mirowsky, J.; Hickey, C.; Horton, L.; Blaustein, M.; Galdanes, K.; Peltier, R.; Chillrud, S.; Chen, L.; Ross, J.; Nadas, A.; Lippmann, M.; Gordon, T. The Effect Of Particle Size, Location And Season On The Toxicity Of Urban And Rural Particulate Matter. *Inhalation Toxicology* 2013, **25 (13)**, 747-757.

23. Charrier, J.; Anastasio, C. On Dithiothreitol (DTT) As A Measure Of Oxidative Potential For Ambient Particles: Evidence For The Importance Of Soluble Transition Metals. *Atmospheric Chemistry and Physics* 2012, **12 (19)**, 9321-9333.

24. Fujitani, Y.; Furuyama, A.; Tanabe, K.; Hirano, S. Comparison Of Oxidative Abilities Of PM2.5 Collected At Traffic And Residential Sites In Japan. Contribution Of Transition Metals And Primary And Secondary Aerosols. *Aerosol and Air Quality Research* 2017, **17 (2)**, 574-587.

25. Software, E. MINEQL+ Chemical Equilibrium Modeling System. https://mineql.com/

26. Lin, M.; Yu, J. Dithiothreitol (DTT) Concentration Effect And Its Implications On The Applicability Of DTT Assay To Evaluate The Oxidative Potential Of Atmospheric Aerosol Samples. *Environmental Pollution* 2019, **251 (0269-7491)**, 938-944.

27. NIST Chemistry WebBook. https://webbook.nist.gov/chemistry/ (accessed Apr 18, 2020).

28. USA, H. DR/890 Portable Colorimeter | Hach USA - Downloads - Obsolete. https://www.hach.com/dr-890-portable-colorimeter/product-downloads?id=7640439041.

29. Barthelmy, D. Bixbyite Mineral Data. http://webmineral.com/data/Bixbyite.shtml#.XpmuMpl7lPY).

30. Verma, V.; Fang, T.; Guo, H.; King, L.; Bates, J.; Peltier, R.; Edgerton, E.; Russell, A.; Weber, R. Reactive Oxygen Species Associated With Water-Soluble PM≪Sub≫2.5≪/Sub≫ In The Southeastern United States: Spatiotemporal Trends And Source Apportionment. *Atmospheric Chemistry and Physics* 2014, **14 (23)**, 12915-12930.

31. Hsu, P. Crystallization Of Iron(III) Phosphate At Room Temperature. *Soil Science Society of America Journal* 1982, **46 (5)**, 928-932.

32. Senn, A.; Kaegi, R.; Hug, S.; Hering, J.; Mangold, S.; Voegelin, A. Composition And Structure Of Fe(III)-Precipitates Formed By Fe(II) Oxidation In Water At Near-Neutral Ph: Interdependent Effects Of Phosphate, Silicate And Ca. *Geochimica et Cosmochimica Acta* 2015, **162**, 220-246.

33. Singh, B.; Gräfe, M. *Synchrotron-based techniques in soils and sediments*; Elsevier, 2010.

34. Lundager Madsen, H.; Koch, C. Kinetics Of Solution Crystal Growth Of Strengite, Fepo4,2H2O. *Journal of Crystal Growth* 2018, **482**, 9-14.

35. Morgan, J.; Stumm, W. *Aquatic chemistry*; Wiley: New York, 1981.

36. Grundl, T.; Delwiche, J. Kinetics Of Ferric Oxyhydroxide Precipitation. *Journal of Contaminant Hydrology* 1993, **14 (1)**, 71-87.

37. Schoonen, M.; Cohn, C.; Roemer, E.; Laffers, R.; Simon, S.; O'Riordan, T. Mineral-Induced Formation Of Reactive Oxygen Species. *Reviews in Mineralogy and Geochemistry* 2006, **64 (1)**, 179-221.

38. Sung, W.; Morgan, J. Kinetics And Product Of Ferrous Iron Oxygenation In Aqueous Systems. *Environmental Science & Technology* 1980, **14 (5)**, 561-568.

39. Faust, S.; Aly, O. *Chemistry of Water Treatment*, 2nd ed.; Taylor & Francis, 1998.

40. Angele Ngantcha-Kwimi, T.; Reed, B. As(V) And PO4 Removal By An Iron-Impregnated Activated Carbon In A Single And Binary Adsorbate System: Experimental And Surface Complexation Modeling Results. *Journal of Environmental Engineering* 2016, **142 (1)**, 04015046.

41. DiStefano, E.; Eiguren-Fernandez, A.; Delfino, R.; Sioutas, C.; Froines, J.; Cho, A. Determination Of Metal-Based Hydroxyl Radical Generating Capacity Of Ambient And Diesel Exhaust Particles. *Inhalation Toxicology* 2009, **21(9)**, 731-738.

42. Lakey, P.; Berkemeier, T.; Tong, H.; Arangio, A.; Lucas, K.; Pöschl, U.; Shiraiwa, M. Chemical Exposure-Response Relationship Between Air Pollutants And Reactive Oxygen Species In The Human Respiratory Tract. *Scientific Reports* 2016, **6 (1)**.

43. Kodavanti, U.; Hauser, R.; Christiani, D.; Meng, Z.; McGee, J.; Ledbetter, A.; Richards, J.; Costa, D. Pulmonary Responses To Oil Fly Ash Particles In The Rat Differ By Virtue Of Their Specific Soluble Metals. *Toxicological Sciences* 1998, **43 (2)**, 204-212.

44. Bell, M.; Ebisu, K.;sss Peng, R.; Samet, J.; Dominici, F. Hospital Admissions And Chemical Composition Of Fine Particle Air Pollution. *American Journal of Respiratory and Critical Care Medicine* 2009, **179 (12)**, 1115-1120.

45. Ostro, B.; Feng, W.; Broadwin, R.; Green, S.; Lipsett, M. The Effects Of Components Of Fine Particulate Air Pollution On Mortality In California: Results From CALFINE. *Environmental Health Perspectives* 2007, **115 (1)**, 13-19.

46. Gonzalez, D.; Cala, C.; Peng, Q.; Paulson, S. HULIS Enhancement Of Hydroxyl Radical Formation From Fe(II): Kinetics Of Fulvic Acid–Fe(II) Complexes In The Presence Of Lung Antioxidants. *Environmental Science & Technology* 2017, **51 (13)**, 7676-7685.

47. Roncal-Herrero, T.; Rodríguez-Blanco, J.; Benning, L.; Oelkers, E. Precipitation Of Iron And Aluminum Phosphates Directly From Aqueous Solution As A Function Of Temperature From 50 To 200 °C. *Crystal Growth & Design* 2009, **9 (12)**, 5197-5205.

48. Bates, J.; Fang, T.; Verma, V.; Zeng, L.; Weber, R.; Tolbert, P.; Abrams, J.; Sarnat, S.; Klein, M.; Mulholland, J.; Russell, A. Review Of Acellular Assays Of Ambient Particulate Matter Oxidative Potential: Methods And Relationships With Composition, Sources, And Health Effects. *Environmental Science & Technology* 2019, **53 (8)**, 4003-4019.

49. T. Burnett, R.; Brook, J.; Dann, T.; Delocla, C.; Philips, O.; Cakmak, S.; Vincent, R.; S. Goldberg, M.; Krewski, D. Association Between Particulate- And Gas-Phase Components Of Urban Air Pollution And Daily Mortality In Eight Canadian Cities. *Inhalation Toxicology* 2000, **12 (suppl 4)**, 15-39.

50. Charrier, J.; McFall, A.; Richards-Henderson, N.; Anastasio, C. Hydrogen Peroxide Formation In A Surrogate Lung Fluid By Transition Metals And Quinones Present In Particulate Matter. *Environmental Science & Technology* 2014, **48 (12)**, 7010-7017.

51. Cho, A.; Sioutas, C.; Miguel, A.; Kumagai, Y.; Schmitz, D.; Singh, M.; Eiguren-Fernandez, A.; Froines, J. Redox Activity Of Airborne Particulate Matter At Different Sites In The Los Angeles Basin. *Environmental Research* 2005, **99 (1)**, 40-47.

52. Dikalov, S.; Griendling, K.; Harrison, D. Measurement Of Reactive Oxygen Species In Cardiovascular Studies. *Hypertension* 2007, **49 (4)**, 717-727.

53. Fang, T.; Verma, V.; Guo, H.; King, L.; Edgerton, E.; Weber, R. A Semiautomated System For Quantifying The Oxidative Potential Of Ambient Particles In Aqueous Extracts Using The Dithiothreitol (DTT) Assay: Results From The Southeastern Center For Air Pollution And Epidemiology (SCAPE). *Atmospheric Measurement Techniques* 2015, **8 (1)**, 471-482.

54. Kawanishi, S.; Oikawa, S.; Inoue, S.; Nishino, K. Distinct Mechanisms Of Oxidative DNA Damage Induced By Carcinogenic Nickel Subsulfide And Nickel Oxides. *Environmental Health Perspectives* 2002, **110 (suppl 5)**, 789-791.

55. Krall, J.; Anderson, G.; Dominici, F.; Bell, M.; Peng, R. Short-Term Exposure To Particulate Matter Constituents And Mortality In A National Study Of U.S. Urban Communities. *Environmental Health Perspectives* 2013, **121 (10)**, 1148-1153.

56. Kramer, A.; Rattanavaraha, W.; Zhang, Z.; Gold, A.; Surratt, J.; Lin, Y. Assessing The Oxidative Potential Of Isoprene-Derived Epoxides And Secondary Organic Aerosol. *Atmospheric Environment* 2016, **130**, 211-218.

57. Laden, F.; Schwartz, J.; Speizer, F.; Dockery, D. Reduction In Fine Particulate Air Pollution And Mortality. *American Journal of Respiratory and Critical Care Medicine* 2006, **173 (6)**, 667-672.

58. Li, N.; Sioutas, C.; Cho, A.; Schmitz, D.; Misra, C.; Sempf, J., M.; Oberley, T.; Froines, J.; Nel, A. Ultrafine Particulate Pollutants Induce Oxidative Stress And Mitochondrial Damage. *Environmental Health Perspectives* 2003, **111 (4)**, 455-460.

59. Li, Q.; Wyatt, A.; Kamens, R. Oxidant Generation And Toxicity Enhancement Of Aged-Diesel Exhaust. *Atmospheric Environment* 2009, **43 (5)**, 1037-1042.

60. Sies, H. Oxidative Stress: Oxidants And Antioxidants. *Experimental Physiology* 1997, **82 (2)**, 291-295.

61. Villamena, F. *Molecular basis of oxidative stress*; John Wiley and Sons, 2013, 22-24.

62. Weichenthal, S.; Shekarrizfard, M.; Traub, A.; Kulka, R.; Al-Rijleh, K.; Anowar, S.; Evans, G.; Hatzopoulou, M. Within-City Spatial Variations In Multiple Measures Of PM2.5 Oxidative Potential In Toronto, Canada. *Environmental Science & Technology* 2019, **53 (5)**, 2799-2810.

63. Xiong, Q.; Yu, H.; Wang, R.; Wei, J.; Verma, V. Rethinking Dithiothreitol-Based Particulate Matter Oxidative Potential: Measuring Dithiothreitol Consumption Versus Reactive Oxygen Species Generation. *Environmental Science & Technology* 2017, **51 (11)**, 6507-6514.

64. Ferreira, C.; Pinto, I.; Soares, E.; Soares, H. (Un)Suitability Of The Use Of pH Buffers In Biological, Biochemical And Environmental Studies And Their Interaction With Metal Ions – A Review. *RSC Advances* 2015, **5 (39)**, 30989-31003.

65. Morgan, J. Kinetics Of Reaction Between O2 And Mn(II) Species In Aqueous Solutions. *Geochimica et Cosmochimica Acta* 2005, **69 (1)**, 35-48.

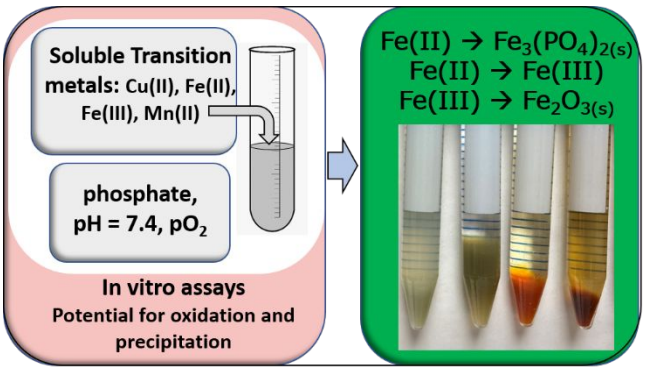

Through macroscopic experiments and thermodynamic modeling, this work demonstrates the precipitation and oxidation of transition metals in phosphate-based *In-vitro* assays.